Supporting Information Cover Sheet

Transformation and Speciation Analysis of Silver Nanoparticles of Dietary Supplement in Simulated Human Gastrointestinal Tract

Wenhao Wu[1], Ruojie Zhang[2], David Julian McClements[2], Benny Chefetz[3], Tamara Polubesova[3], Baoshan Xing[1,*]

[1]Stockbridge School of Agriculture, University of Massachusetts, Amherst, MA 01003, USA

[2]Department of Food Science, University of Massachusetts, Amherst, MA 01003, USA

[3]Department of Soil and Water Sciences, Hebrew University of Jerusalem, Rehovot 76100, Israel

*Corresponding Author: Dr. Baoshan Xing, Phone: 413-545-5212, Email: bx@umass.edu

Number of pages: 13

Number of tables: 2

Number of figures: 6

Journal: *Environmental Science & Technology*

Date prepared: June 2, 2018

Table S1. Composition of gastrointestinal fluids in human gastrointestinal tract model (g/L, T=37^{o}C)

Saliva (pH=6.8)		**Gastric fluid (pH=2.5)**			**Small intestinal fluid (pH=7.0)**		
			Fasted	**Fed**		**Fasted**	**Fed**
NaCl	2.0	NaCl	2.0	2.0	NaCl	52.6	52.6
mucin	3.0	pepsin	0.4	3.2	bile salts	3.0	30.0
α-amylase	0.5	mucin	3.0	3.0	pancreatin	2.4	14.4

Notes:

1. A few insoluble impurities in the prepared gastrointestinal fluids were removed by centrifuge before mixing with AgDS for better analysis of AgNPs by UV-Visible spectroscopy.

2. Volumes of AgDS and gastrointestinal fluids in the digestion.
Mouth phase: AgDS (15mL) + saliva (15mL)
Stomach phase: “bolus” from mouth phase (15mL) + gastric fluid (15mL)
Small intestine phase: “chyme” from stomach phase (25mL) + small intestinal fluid (5mL)

3. The used products of mucin, α-amylase, pepsin, pancreatin and bile salts in the simulated GIT are all from pigs, because (i) the structures and activities of these gastrointestinal components from pigs are similar with that from humans; (ii) these gastrointestinal components from humans are much more expensive and extremely difficult to obtain as compared with that from pigs; and (iii) many simulated GIT models used the gastrointestinal components from pigs (*1-3*). The concentrations of the gastrointestinal components and residence times were set according to the previous studies, which were similar to the human GIT (*1-3*).

Table S2. Ingredients of the AgDS Product

Ingredients	Concentration (mg/L)	Ingredients	Concentration (mg/L)
AgNPs	17.96±0.09[a]	Ag^+	8.00±0.03[a]
Na^+	0.012±0.005[a]	Cl^-	0.010±0.005[b]
K^+	ND[a]	NO_3^-	0.024±0.010[b]
Mg^{2+}	ND[a]	SO_4^{2-}	ND[b]
Ca^{2+}	ND[a]	$H_2PO_4^{3-}$	ND[b]
Fe^{2+}/Fe^{3+}	ND[a]	TOC	0.58±0.08[c]
Al^{3+}	ND[a]	IC	ND[c]

Note: The pH of the AgDS is 5.8±0.1 as measured by a pH meter (Accumet XL200, Fisher); [a]Data were detected by Inductively Coupled Plasma Mass Spectrometry (ICPMS-2030, Shimadzu), AgNPs and Ag^+ were separated by centrifugal filter devices (Amicon Ultra-4 3K) as mentioned in the text, and HNO_3 digestion was conducted before detection; [b]Data were detected by Ion Chromatography (Dionex, Thermo Scientific); [c]Total Organic Carbon (TOC) and Inorganic Carbon (IC) were detected by Total Organic Carbon Analyzer (TOC-L, Shimadzu); ND: Not Detectable; Duplicate were conducted.

The limitations of DLS, SP-ICPMS and SAXS in characterization of AgNPs from AgDS in the simulated gastrointestinal tract.

The Dynamic Light Scattering (DLS) is a widely used method to characterize the particle size distribution and aggregation of nanoparticles in simple aqueous solution (*4*). Unfortunately, this method can be poorly applied for nanoparticles in the complex medium, due to the reasons that the DLS method calculating the average particle size can provide misleading results by a few large particles in a mixture and it also cannot differentiate different particles in a mixture (*5,6*). In this study, the hydrodynamic diameter of AgNPs in the AgDS determined by DLS is 32.6±9.4 nm (Figure 1B), while the hydrodynamic diameters of the colloidal biomolecules in all simulated digestive fluids are >200 nm. Thus, the DLS cannot be used to characterize the AgNP aggregation in the simulated gastrointestinal tract. The Single-particle ICPMS (SP-ICPMS) is a novel method to characterize the particle size distribution, aggregation and dissolution of metal nanoparticles in complex medium (*5*). However, the SP-ICPMS is also not feasible to be applied in this study, because the core size of AgNP from AgDS, i.e., 14.0±2.5 nm (TEM, Figure 1A), is lower than the size detection limit of SP-ICPMS for AgNPs, i.e., 18-20 nm (*5*). The Small Angle X-ray Scattering (SAXS) can also be used to detect the particle size distribution, aggregation and dissolution of AgNPs in complex medium, because the SAXS intensity of metal nanoparticles are much higher than that of biomolecules and the SAXS intensity of background solution containing biomolecules could be negligible for AgNPs (*7-10*). However, synchrotron X-ray beamline and high AgNP concentration are required for obtaining reliable results (*7-10*), where the former is available only in the national lab equipped with synchrotron radiation facilities and the latter is not feasible in this study. Despite the limitations of the SAXS method, we prolonged the measurement time in order to enhance the

reliability of SAXS results. SAXS results of original AgDS suspension and the AgDS in saliva were obtained through 2-hours measurement and displayed in Figure S1, however, SAXS results of AgDS in gastric and small intestinal fluid were not acceptable, due to the continually dissolution of AgNPs in the 2-hours measurement and too low concentrations of AgNPs in both gastric and small intestinal fluids.

SAXS method and the SAXS results of AgDS and AgDS in Saliva.

The AgDS samples were filled in quartz capillary tubes and measured on a SAXSLAB Ganesha instrument with Cu *K*α 0.154 nm line on SAXS or ESAXS mode. The measured intensity was corrected by subtracting the intensity of a capillary filled with pure water, and then fitted with Lognormal equation using the Igor pro 6.37 software with an Irena program to obtain the particle size distribution of AgNPs.

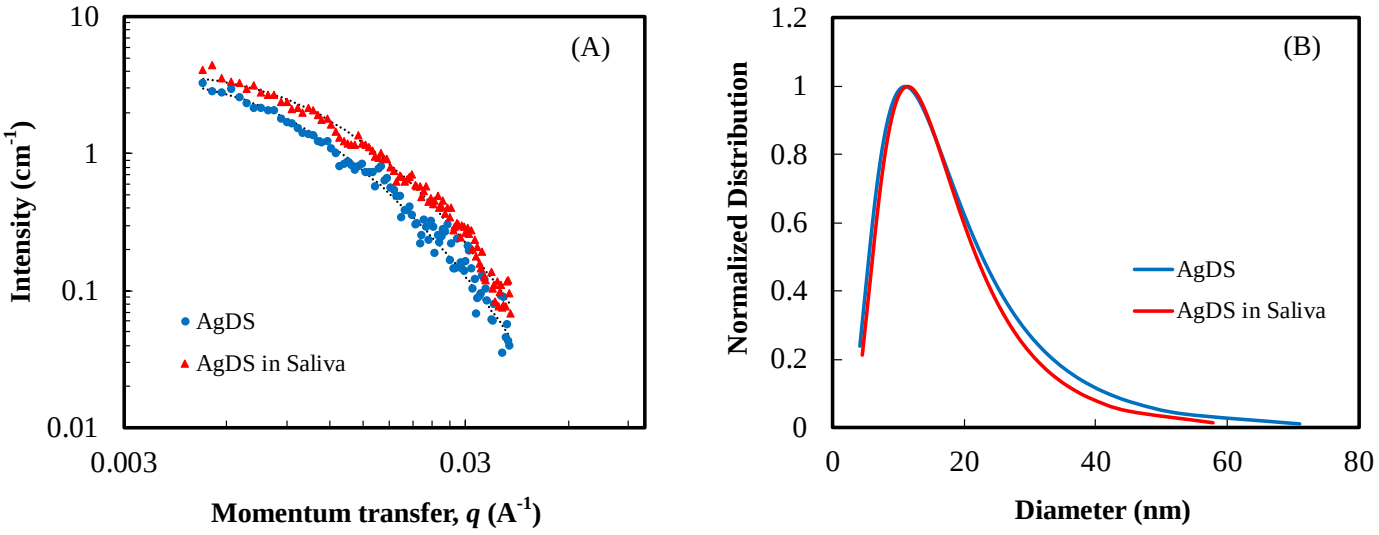

Figure S1. Small Angle X-ray Scattering data and Lognormal-fitted results (dash curves) of original AgDS suspension and the AgDS in saliva (A) and the calculated particle size distributions based on Lognormal distribution (B). The data fitting and calculation were conducted using the Igor pro 6.37 software with an Irena program. The mean diameter and standard deviation of AgDS is 15.7±4.4 nm, while that of AgDS in saliva is 15.1±3.7 nm.

Evidence for no AgNPs-AgCl core-shell structure being formed in the simulated GIT.

According to the Drude model of the electronic structure of metals (*11*), the Localized Surface Plasmon Resonance (LSPR) peak wavelength increases with the refractive index of the medium.

$$\lambda_{max} = \lambda_p (2n_m^2+1)^{0.5}$$

where λ_{max} is the LSPR peak wavelength, λ_p is the wavelength corresponding to the plasma frequency of the metal and n_m is the refractive index of the medium (*11*). The refractive indexes of AgCl (2.07) are much higher than that of the simulated GIT (1.36~1.60) (*11-13*). Thus, if the AgNPs-AgCl core-shell structure was formed in the simulated GIT, its peak wavelength should increase accordingly. From the silver speciation results of the AgDS in the simulated GIT (Table 1), AgCl was only formed in the stomach phase. However, the peak wavelength of AgDS in the 2-hour stomach phase kept constant (Figures 3A and 3B). Therefore, AgNPs-AgCl core-shell structure was not formed in the stomach phase and further in the whole simulated GIT.

Schematic Method Flow of the Silver Speciation Analysis

First, Ag^+ ($AgNO_3$) with a series of known concentrations (0, 5, 10, 15, 20 and 25 mg/L) were passed through the simulated gastrointestinal tract. Mouth phase: Ag^+ (15mL) + saliva (15mL); stomach phase: "bolus" from mouth phase (15mL) + gastric fluid (15mL); small intestine phase: "chyme" from stomach phase (25mL) + small intestinal fluid (5mL).

Second, the schematic flow of silver speciation analysis for the obtained digesta fluids is displayed below.

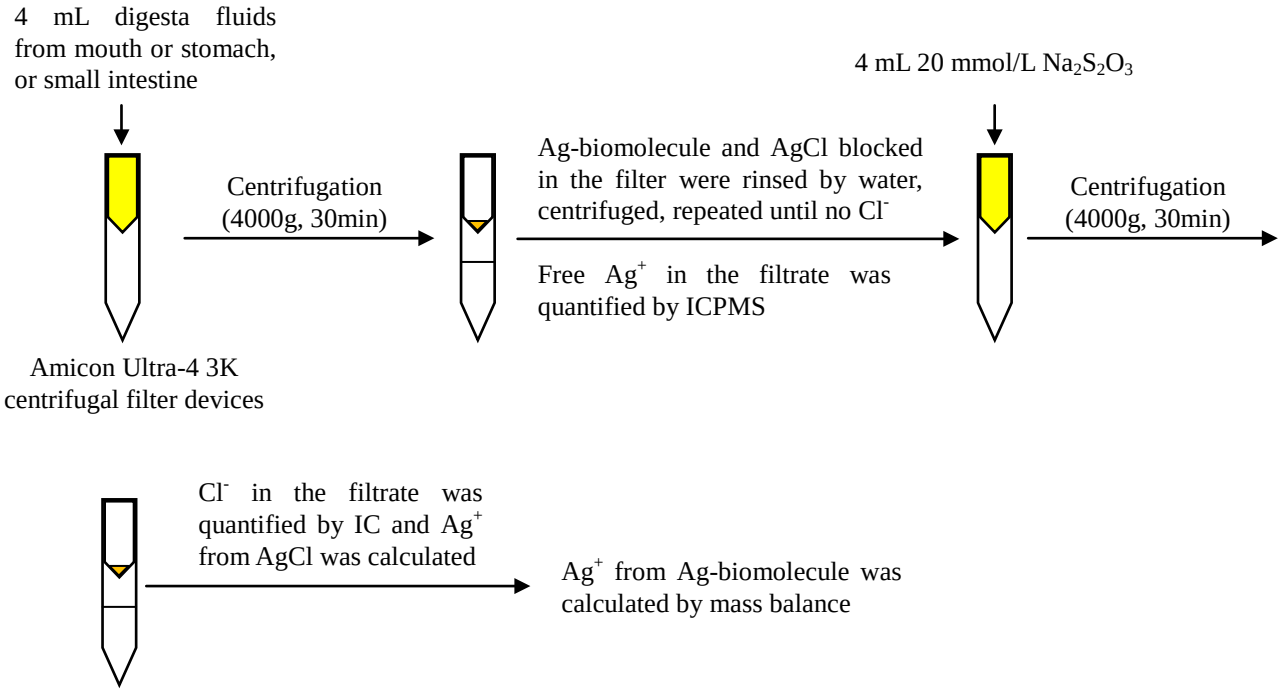

Figure S2. Schematic flow of the Silver Speciation Analysis

Third, the quantitative relationship between the total silver ion concentration in the gastrointestinal fluids and the concentrations/distributions of different silver ion species was established. Please see Figure 4A.

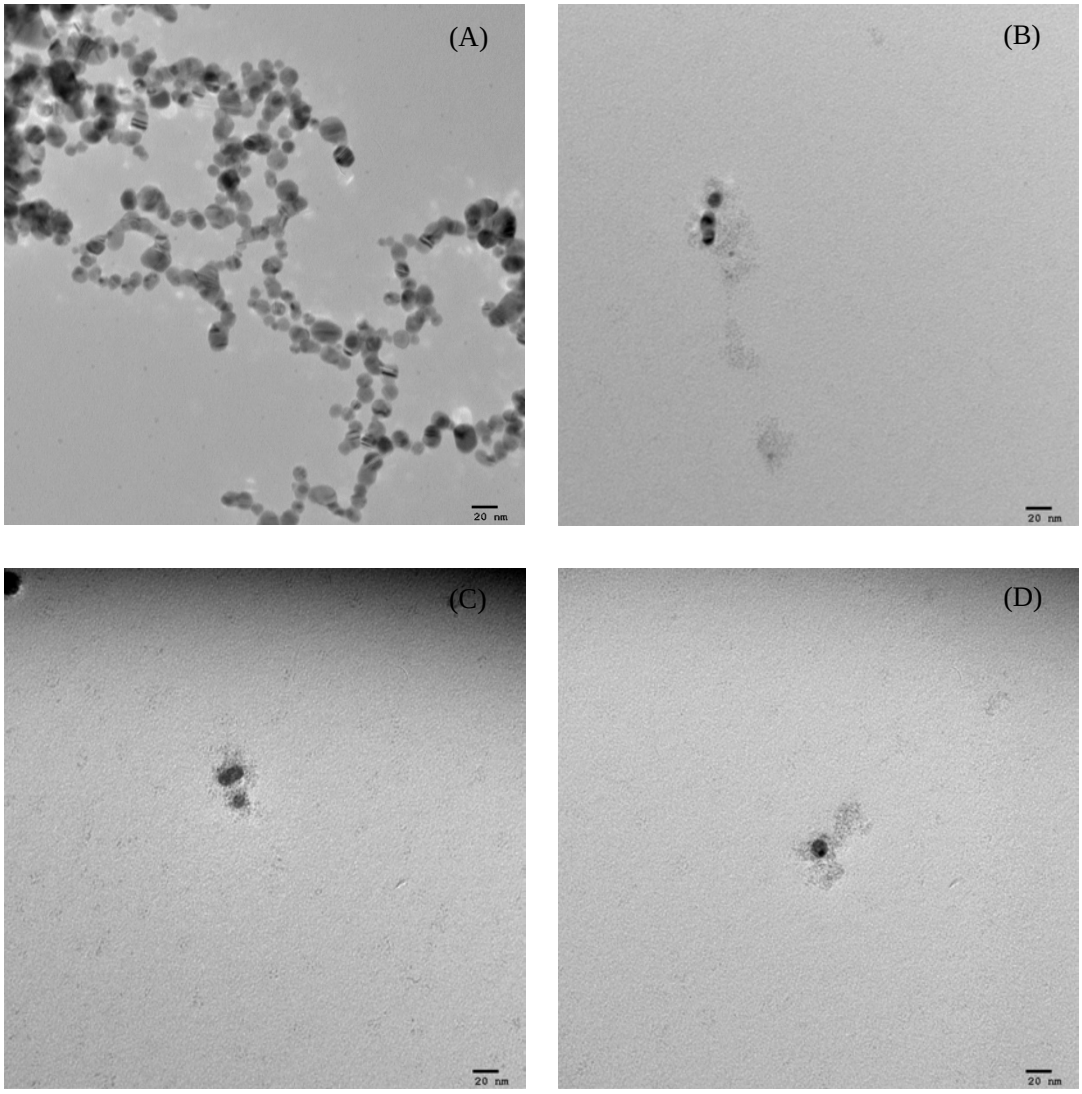

Figure S3. TEM images of AgDS (A), AgDS in the mouth phase (B), AgDS in the stomach phase (C), and AgDS in the small intestine phase (D). The TEM samples in the simulated GIT (B, C, D) were stained by 1% uranyl acetate, in order to see the biomolecular corona. The shadows surrounding AgNPs are the biomolecular corona.

Effects of biomolecules on the maximum adsorption wavelength (λ_{max}) of AgDS.

In order to verify the role of biomolecules in the redshift of the λ_{max} of AgDS, the saliva biomolecule concentration was diluted to 0.03, 0.06, 0.10, 0.30, 0.60 times of its original concentration, while the ionic strength was kept constant (2 g/L). AgDS was mixed respectively with the saliva containing different biomolecule concentrations, and the corresponding UV-Vis spectra of AgDS are displayed in Figure S4. The redshift of the λ_{max} of AgDS increased as the saliva biomolecule concentration increased, demonstrating that the binding of biomolecules on the AgNPs is responsible to the redshift. The biomolecular corona around AgNPs can be clearly seen from the TEM images (Figures S3).

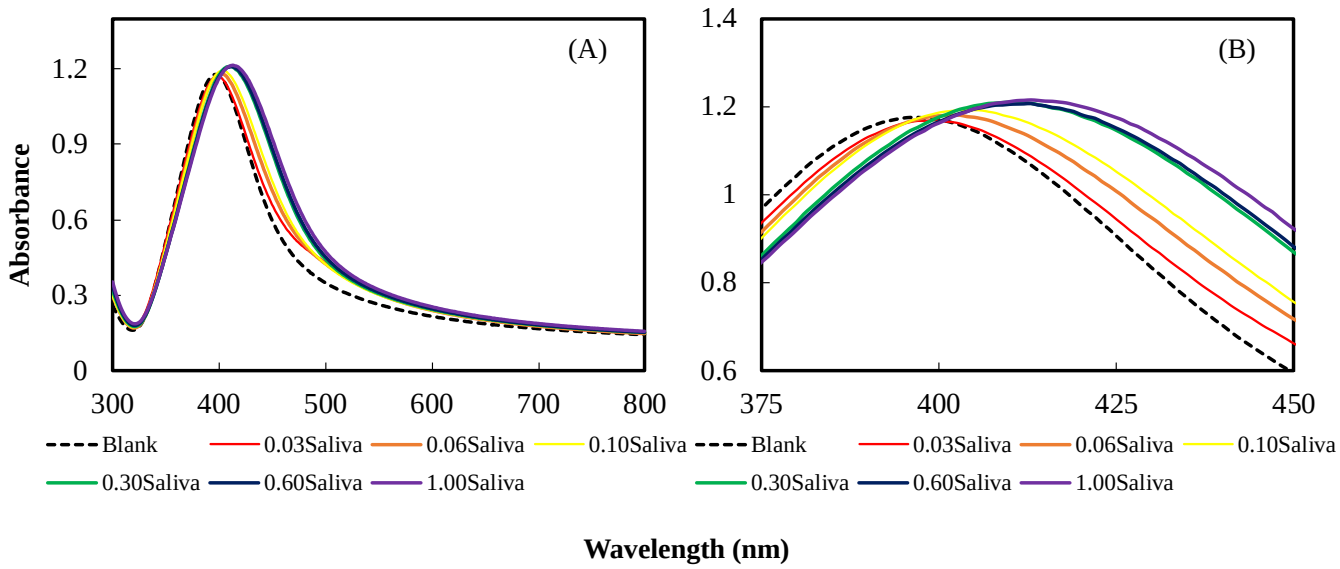

Figure S4. UV-Vis spectra of AgDS in saliva containing biomolecules with 0.03, 0.06, 0.10, 0.30, 0.60, and 1.00 times of its original concentration and 2 g/L NaCl. Both background and dilution corrections were conducted. The redshift of the λ_{max} of AgDS increased as the biomolecule concentration increased (Panel B is magnified from panel A).

Effects of ionic strength on the maximum adsorption wavelength (λ_{max}) of AgDS.

In order to verify the effect of NaCl on the redshift of the λ_{max} of AgDS, the NaCl concentrations were set as 0, 0.2, 0.5, 1.0, 1.5, 2.0 g/L, while the saliva biomolecule concentration was kept constant (0.10 time of its original concentration). AgDS was mixed respectively with the saliva containing different NaCl concentrations, and the corresponding UV-Vis spectra of AgDS are displayed in Figure S5. The redshift of the λ_{max} of AgDS decreased as the NaCl concentration increased, indicating that the increasing NaCl concentration in solution can reduce the redshift caused by biomolecules.

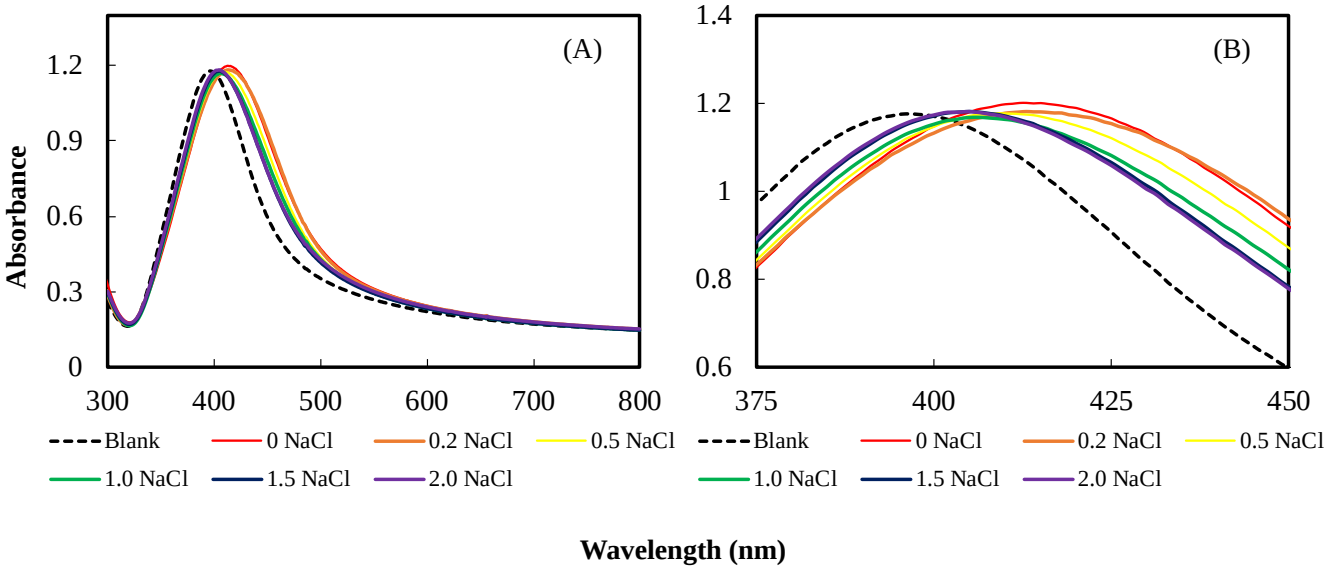

Figure S5. UV-Vis spectra of AgDS in saliva containing 0, 0.2, 0.5, 1.0, 1.5, 2.0 g/L NaCl and biomolecules with 0.10 time of its original concentration. Both background and dilution corrections were conducted. The redshift of the λ_{max} of AgDS reduced as the NaCl concentration increased (Panel B is magnified from panel A).

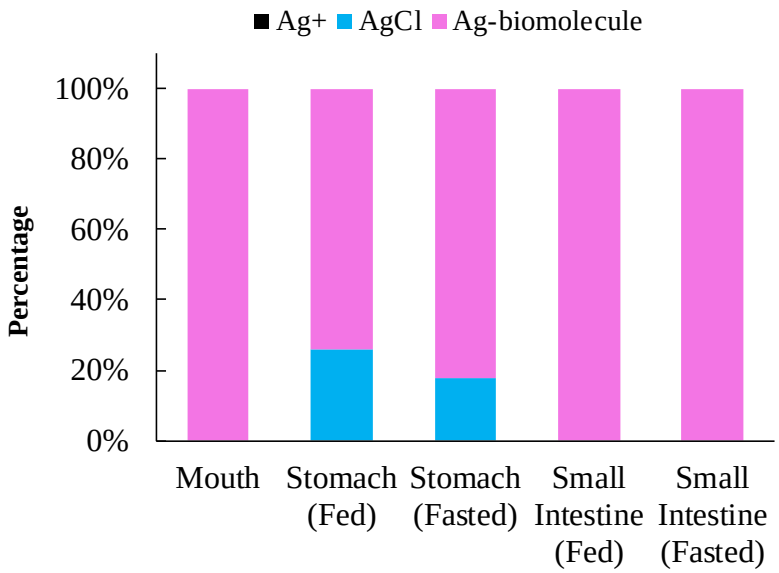

Figure S6. Percentages of silver ion species from AgDS in the simulated gastrointestinal tract.

References

[1] Zhang, R.; Wu, W.; Zhang, Z.; Park, Y.; He, L.;Xing, B.; McClements, D.J. Effect of the composition and structure of excipient emulsion on the bioaccessibility of pesticide residue in agricultural products. *J. Agric. Food Chem.* **2017**, 65(41), 9128-9138.

[2] Minekus, M.; Alminger, M.; Alvito, P.; Ballance, S.; Bohn, T.; Bourlieu, C.; Carrière, F. ; Boutrou, R.; Corredig, M.; Dupont, D.; Dufour, C.; Egger, L.; Golding, M.; Karakaya, S.; Kirkhus, B.; Le Feunteun, S.; Lesmes, U.; Macierzanka, A.; Mackie, A.; Marze, S.; McClements, D.J.; Ménard, O.; Recio, I.; Santos, C.N.; Singh, R.P.; Vegarud, G.E.; Wickham, M.S.J.; Weitschies, W.; Brodkorb A. A standardised static in vitro digestion method suitable for food – an international consensus. *Food Funct.* **2014**, 5, 1113-1124.

[3] Wang, Z.; Zhao, J.; Song, L.; Mashayekhi, H.; Chefetz, B.; Xing, B. Adsorption and desorption of phenanthrene on carbon nanotubes in simulated gastrointestinal fluids. *Environ. Sci. Technol.* **2011**, 45(14), 6018-6024.

[4] Levard, C.; Hotze, E.M.; Lowry, G.V.; Brown, G.E. Environmental transformations of silver nanoparticles: Impact on stability and toxicity. *Environ. Sci. Technol.* **2012**, 46(13), 6900-6914.

[5] Walczak, A.P.; Fokkink, R.; Peters, R.; Tromp, P.; Herrera Rivera, Z.E.; Rietjens, I. M.; Hendriksen, P.J.; Bouwmeester, H. Behaviour of silver nanoparticles and silver ions in an in vitro human gastrointestinal digestion model. *Nanotoxicology* **2013**, 7(7), 1198-1210.

[6] Mehrabi, K.; Nowack, B.; Dasilva, Y.A.R.; Mitrano, D.M. Improvements in nanopaticle tracking analysis to measure particle aggregation and mass distribution: A case study on engineered nanomaterial stability in incineration landfill leachates. *Environ. Sci. Technol.* **2017**, 51, 5611-5621.

[7] Kastner, C.; Lichtenstein, D.; Lampen, A.; Thunemann, A.F. Monitoring the fate of small silver nanoparticles during artificial digestion. *Colloids and Surfaces A: Physicochem. Eng. Aspects* **2017**, 526, 76-81.

[8] Bohmert, L.; Girod, M.; Hansen, U.; Maul, R.; Knappe, P.; Niemann, B.; Weidner, S.M.; Thunemann, A.F.; Lampen, A. Analytically monitored digestion of silver nanoparticles and their toxicity on human intestinal cells. *Nanotoxicology* **2014**, 8(6), 631-642.

[9] Martin, M.N.; Allen, A.J.; MacCuspie, R.I.; Hackley, V.A. Dissolution, agglomerate

morphology, and stability limits of protein-coated silver nanopartilces. *Langmuir* **2014**, 30, 11442-11452.

[10] Li, T.; Senesi, A.J.; Lee, B. Small angle X-ray scattering for nanoparticle research. *Chem. Rev.* **2016**, 116(18), 11128–11180.

[11] Mayer, K.M.; Hafner, J.H. Localized surface plasmon resonance sensors. *Chem. Rev.* **2011**, 111, 3828-3857.

[12] Hilton, L.W.; Plyler, E.K.; Stephens, R.E. Refractive index of silver chloride for visible and infra-red radiant energy. *J. Opt. Soc. Am.* **1950**, 40(8), 540-543.

[13] Miclaus, T.; Bochenkov, V.E.; Ogaki, R.; Howard, K.A.; Sutherland, D.S. Spatial mapping and quantification of soft and hard protein coronas at silver nanocubes. *Nano Lett.* **2014**, 14(4), 2086-2093.